RSC Advances

PAPER

View Article Online
View Journal | View Issue

Cite this: *RSC Adv.*, 2014, **4**, 44480

Au nanoparticle-loaded PDMAEMA brush grafted graphene oxide hybrid systems for thermally smart catalysis†

Jing Chen,[a] Peng Xiao,[a] Jincui Gu,[a] Youju Huang,*[a] Jiawei Zhang,[a] Wenqin Wang[b] and Tao Chen*[a]

Received 11th June 2014
Accepted 2nd September 2014

DOI: 10.1039/c4ra05592f

www.rsc.org/advances

A novel smart catalytic system was successfully constructed by using poly[(dimethylamino)ethyl methacrylate] (PDMAEMA) brush grafted graphene oxide (GO) to load gold nanoparticles (Au NPs). The catalytic activity of the Au NPs was finely tuned by temperature, which can control the inclusion and 'exposure' of Au NPs inside the PDMAEMA brushes *via* the phase transition of the grafted PDMAEMA chain triggered by a temperature above the lower critical solution temperature (LCST) of PDMAEMA.

Introduction

Graphene, a single atomic layer of a carbon network, has been highlighted as a novel two-dimensional material because of its unique mechanical, optical, and electrical properties.[1–6] In addition to the various application explorations of graphene in electronic and energy storage devices, biomedical devices, and ultrathin membranes,[7–11] it also has been considered as a promising support for heterogeneous catalysis due to its large surface area with outstanding mechanical and electronic transfer properties. Due to the surface abundant functionality, graphene oxide (GO) and sulfonated graphene have been the focus particularly as catalysis support.[12–19] For example, Gupta *et al.*[20] developed a novel catalyst based on Fe@Au bimetallic nanoparticles (NPs) involved graphene oxide. This nanocatalyst was stable, recyclable and showed excellent catalytic activity. Liu *et al.*[21] found that a novel york/shell Fe_3O_4@PDA/RGO/Pt exhibited high electrochemical activity and stability to methanol oxidation, which was attributed to the synergetic cocatalytic effect at the heterojunction interfaces between the Pt nanoparticles and the support. Loh *et al.*[22] showed a composite made from the assembly of GO and copper-centered metal organic framework (MOF), which showed good performance as a tri-functional catalyst in three important electrocatalysis reactions.

With this in mind, numerous studies have focused on the exploration of tunable catalyst systems.[23] Ballauff demonstrated a thermosensitive poly(*N*-isopropylacrylamide) (PNIPAM) network grafted polystyrene (PS) sphere can act as a "nanoreactor" that can be opened or closed to a certain extent where the catalytic activity of the silver NPs inside PNIPAAM network can be modulated by temperature over a wide range.[24] Graphene supported nanocatalysts with smart adjustable catalytic behavior is still extremely desirable and remains a challenge. Recently, Fan and co-workers[25] demonstrated a unique graphene-based smart catalytic system which consists of the graphene supported Au–Pt bimetallic nanocatalyst and a dextran-based temperature-responsive polymer. The catalytic activities were readily tunable based on the temperature responsibility of the polymer. However, the metallic NPs were usually deposited on the GO supports by adsorption, which lead to a limited loading. To solve these problems, it is important to anchor metallic NPs firmly on the carrier surface.

Recently, it had been demonstrated that polymer brushes can be introduced to GO through various polymerization method,[26–28] particularly, polymer brushes can be prepared even without a surface-bound initiator by SIPGP on self-assembled monolayers (SAMs).[29,30] As a photo active site, –OH group on GO could be initiated to grow polymer brushes by self-initiated photografting and photopolymerization (SIPGP) from GO films without a surface bonded initiator.[31] The grafted polymer brushes could significantly improve the loading of the immobilized metallic NPs, which enhance the catalytic activities.

In this paper, we report a hybrid catalysis system made of exfoliated GO grafted by PDMAEMA brushes with a subsequent loading of Au NPs. This unique catalytic system is prepared by introducing PDMAEMA to GO through SIPGP,[32] followed by direct co-reduction to obtain the GO@PDMAEMA/Au hybrid system with coordinate linkages to the Au NPs. The temperature responsibility of PDMAEMA brushes endows the hybrid catalysis system with the expected thermo-sensitive catalytic activities.

[a]*Division of Polymer and Composite Materials, Ningbo Institute of Material Technology and Engineering, Chinese Academy of Science, Ningbo 315201, China. E-mail: tao.chen@nimte.ac.cn; yjhuang@nimte.ac.cn*

[b]*Faculty of Materials Science and Chemical Engineering, Ningbo University, Ningbo 315211, China*

† Electronic supplementary information (ESI) available. See DOI: 10.1039/c4ra05592f

Experimental

Materials

All chemicals were analytical grade or of the highest purity available. Expandable graphite was purchased from Qingdao BCSM Co., Ltd. $HAuCl_4$, $NaBH_4$ and 4-nitrophenol were purchased from Sinopharm Chemical Reagent Co., Ltd. and used as received. 2-dimethylaminoethyl methacrylate (DMAEMA) was purchased from the Energy Chemical Company. All other reagents were purchased from commercial sources and used as received.

Preparation of graphene oxide aqueous solution

Graphene oxide (GO) sheets were synthesized by a modified Hummers' method[33] and exfoliation of graphite oxide was achieved by a strong ultrasonication method. The obtained brown dispersion was then washed and centrifuged to remove any unexfoliated graphite oxide. The final GO nanosheets with diameter were less than 2 μm, which was used for next process.

SIPGP

1 mg mL^{-1} of GO aqueous solution and 2 mL of monomer (DMAEMA) were added into a tube. The tube was placed under a UV lamp and irradiated for 40 min at room temperature. A high-pressure mercury lamp from Jiguang Co. (Shanghai, China) was used for SIPGP. Its wavelength ranged from 200 to 400 nm. The distance between the reaction mixture and the light source was 10 cm. To remove the ungrafted polymer, the precipitate was dispersed in acetone and centrifuged at 8000 rpm for three times. The black polymer-grafted GO was collected and dried in vacuum at 80 °C for 24 h before characterization.

GO@PDMAEMA for loading the gold NPs

The details of loading the gold NPs were as following: 50 mg of GO@PDMAEMA were first dispersed in 10 mL of deionized water and then 0.25 mL of 4 mM $HAuCl_4$ aqueous solution was added. The reaction lasted for 1 h after adding 1 mL of 0.05 M $NaBH_4$ aqueous solution dropwise under the ice water bath with shaking. The final product was purified through washing with water three times and dried under vacuum oven until constant weight.

Catalytic reduction of 4-nitrophenol to 4-aminophenol in an aqueous medium

A typical experiment for the catalytic reduction of 4-nitrophenol (4-NP) to 4-aminophenol (4-AP) was carried out as follows: 0.1 mL of 4-NP aqueous solution (5 mM, 5×10^{-7} mol), 1.0 mL of $NaBH_4$ (0.2 M, 2×10^{-4} mol) aqueous solution and 2.0 mL of water were mixed in a colorimetric tube. We introduced 0.05 mL of catalyst dispersion (1.0 mg mL^{-1}) into the mixture with gentle shaking. The bright-yellow solution faded gradually as the catalytic reaction proceeded. The catalytic activity was determined by a UV-vis spectrophotometer with a decrease at 400 nm in UV-vis absorbance and a simultaneous increase in the absorption at 300 nm, indicating the formation of 4-AP.

Characterizations

The GO and GO@PDMAEMA were characterized by atomic force microscopy (CSPM 5500) in tapping mode. The spring constant of scanning probes is 40 N m^{-1}. Fourier transform infrared (FTIR) Spectroscopy (Nicolet 6700, Thermoscientific, USA): the spectra were measured with a spectrometer. Absorbance spectra were collected using a spectral resolution of 4 cm^{-1} at room temperature over a frequency range of 4000–500 cm^{-1}. The background spectra were recorded on corresponding KBr. Thermogravimetric analysis (TGA) was carried out on a METTLER TOLEDO-TGA/DSC I instrument with a heating rate of 10 °C min^{-1} in flowing N_2 and a sample of 3–5 mg. The morphology and size of the samples were investigated using transmission electron microscopy (TEM, Tecnai F20 S-TWIN (FEI), accelerating voltage of 200 kV). TEM samples were prepared by dropping a diluted aqueous solution (5 μL) of samples onto carbon-coated copper grids and were dried in air for 1 h. UV-vis absorption spectra of the samples were recorded using a Lambda 950 spectrophotometer (Perkin-Elmer). Measurements of the solutions were taken in 3 mL quartz cuvettes. Dynamic light scattering (DLS) analysis was performed using a Malvern Zetasizer Nano instrument with a laser light wavelength of 633 nm, and all data were averaged over three measurements. X-ray Photoelectron spectrum (XPS) (AXIS ULTRA DLD, Kratos Analytical Ltd., Manchester, UK) measurements were carried out at pressures between 10^{-9} and 10^{-8} mbar. All peaks are referenced to the signature of the C 1s peak for carbon at 284.8 eV, The XPS system was equipped with a monochromatic Al Kα source.

Results and discussion

This unique smart catalytic system was composed of graphene supported temperature-responsive polymer and Au nanocatalyst *via* the coordination of the amino groups of PDMAEMA with gold atoms (Scheme 1). In brief, SIPGP was first used to graft PDMAEMA from GO.[31] The Au NPs were then facilely

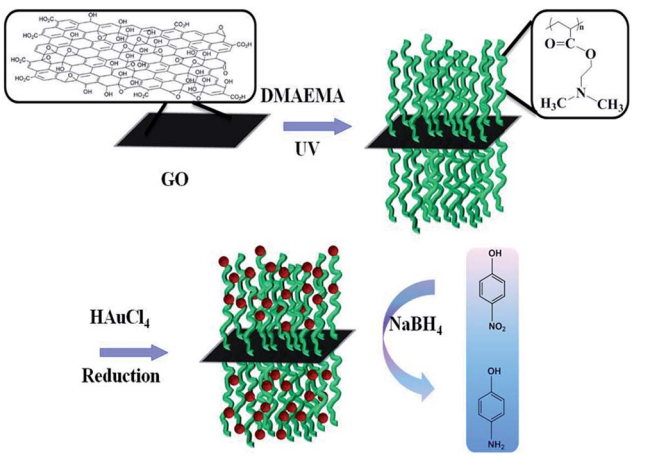

Scheme 1 Schematic representation of GO@PDMAEMA/Au hybrid system consisting of thermosensitive polymer in which Au NPs are loaded.

loaded onto the thermosensitive PDMAEMA brushes through *in situ* reduction of $HAuCl_4$ using $NaBH_4$ as a reductant. The thermoadjustable catalytic activity at various temperatures of the hybrid system was finally investigated.

The preparation process of the GO@PDMAEMA/Au hybrid system was recorded by transmission electron microscopy (TEM). The transparent and creased GO nanosheet exhibited mono- or few layer planar sheets (Fig. 1A). Thermal responsive PDMAEMA with a lower critical solution temperature (LCST) at ~40 °C was subsequently grafted onto the GO by SIPGP. It is obviously to see that GO@PDMAEMA (Fig. 1B) displayed thick plates with dark contrast, indicating the reminiscent of the polymeric structures on the GO nanosheet. FT-IR spectroscopy (Fig. S1†) was also used to further confirm the successful functionalization of the GO sheet with PDMAEMA brushes. Owing to the incorporation of thermorsensitive PDMAEMA component, the polymer-grafted GO sheets can be readily dissolved in water with the aid of moderate sonication and also exhibit typical temperature-responsive association behavior. The size distribution of thermoresponsive GO@PDMAEMA from 15 to 60 °C in aqueous solution was characterized by dynamic light scattering (DLS) (Fig. S2†). It was shown that the average size (around 2.0 μm) due to remarkable aggregation was firstly obtained below 30 °C, but that the size decreases to 400 nm near 42 °C. The decrease of composites size can be ascribed to the collapse of PDMAEMA upon heating. Thermogravimetric analysis (TGA) (Fig. 1C and S3†) was carried out to study the thermal stability and the grafting density of the composites. The GO was found to have a 70 wt% weight loss in the range of 100–800 °C, due to the thermal decomposition of oxygen-containing groups.[32,33] Pure PDMAEMA exhibited two distinct weight loss steps: one was at a range of 150–300 °C arising from the thermal decomposition of remaining oxygen-containing groups; the other was at a range of 300–550 °C caused by the thermal decomposition of polymer backbones. The GO@PDMAEMA nanocomposite showed 87% weight loss, indicating the weight percentage of PDMAEMA was about 17%.

The X-ray photon spectroscopy (XPS) spectrum provided information on the type and number of different species of a given atom in the molecules. GO and GO@PDMAEMA were characterized by XPS (Fig. 2). For GO@PDMAEMA, there was a peak at 399.8 eV corresponding to the N1s binding energy of PDMAEMA chains. However, the XPS spectrum of GO didn't show a peak at 399.8 eV, which implied that the surfaces of the flakes of GO@PDMAEMA had been successfully functionalized with PDMAEMA. The corresponding C1s binding energy of GO

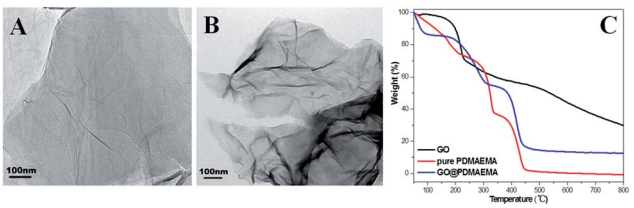

Fig. 1 TEM images: (A) pure GO, (B) GO@PDMAEMA and (C) TGA spectra of (black) GO, (red) pure PDMAEMA, (blue) GO@PDMAEMA.

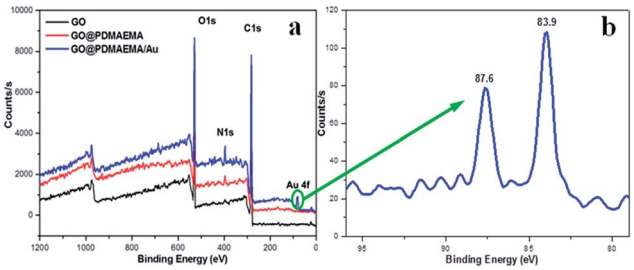

Fig. 2 (a) XPS survey spectra of the GO, GO@PDMAEMA and GO@PDMAEMA/Au and (b) Au 4f XPS spectra of smart GO@PDMAEMA/Au system.

and GO@PDMAEMA nanocomposite were also shown in Fig. S4.† The C1s XPS spectrum of GO showed binding energies at 284.6 eV (C–C in GO), 286.3 eV(C–O), 287 eV (C═O), and 288.3 eV(O–C═O). The C1s XPS spectrum of GO@PDMAEMA nanocomposite also showed all the energy peaks of C1s, but the percentage of the area of the peak at 288.3 eV (O–C═O) increased from 0.54% to 10.88%, which also proves the grafting of PDMAEMA chains onto the surface of GO sheets.

Au NPs were deposited onto the GO@PDMAEMA by *in situ* reduction of $HAuCl_4$ using $NaBH_4$. The abundant tertiary amino groups of PDMAEMA brushes could serve as good linkers to strongly interact with Au NPs. From XPS result demonstrated in Fig. 2, the Au $4f_{7/2}$ and Au $4f_{5/2}$ peaks appeared at 83.9 eV and 87.6 eV, respectively, which were in accordance with the characteristic peaks for the metallic Au^0 state,[34] verifying again the success of Au NPs modification on the GO@PDMAEMA. In order to corroborate residual weight is only due to the gold present in the samples, TGA and DTG analysis of core–shell composites before loading Au NPs (black) and after loading Au NPs (red) were made (Fig. S3†). These two distinct weight loss stages of GO@PDMAEMA and GO@PDMAEMA/Au between 200 and 500 °C are very similar, which illustrates that GO@PDMAEMA/Au hybrid system remained high thermostability.

The TEM images of GO@PDMAEMA/Au (Fig. 3A and B) show that the tiny gold nanocolloids were well-dispersed in the outer PDMAEMA brushes without any aggregation. A HRTEM image of the Au NPs was presented in the right-top inset of Fig. 3B. It showed that Au NPs were relatively uniform with diameters around 2–3 nm and the lattice fringes with a lattice spacing of about 0.235 nm were corresponding to the (111) plane of face center cubic (fcc) structure of Au NPs. Moreover, there were nearly no isolated Au nanoparticles separately from the GO@PDMAEMA, due to the strong interaction between the Au NPs and GO@PDMAEMA. Elements C, O, N and Au were found in the energy dispersive X-ray spectroscopy (EDX) mapping (Fig. 3C) of the GO@PDMAEMA/Au hybrid, which confirmed that Au NPs were homogeneously distributed in the hybrid system. To solve the overdosage of noble metal Au and further lower the cost of catalysts, comparison experiments of different loading of Au were also supplemented in this work. From Fig. S5,† we can conclude that the optimal concentration of Au^{3+} is 4 mM, just used in our hybrid system.

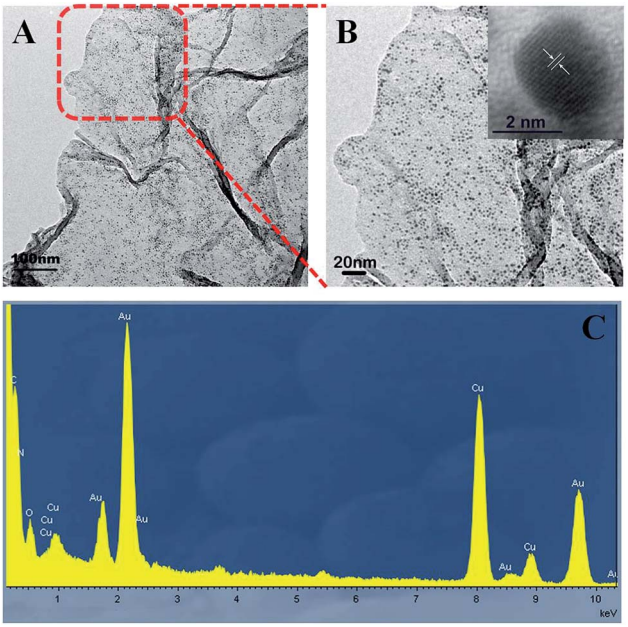

Fig. 3 (A and B) TEM images of GO@PDMAEMA/Au. The right-top inset shown in (B) presents a HRTEM image of an Au NP. (C) EDX spectrum of GO@PDMAEMA/Au. The copper peaks are from the copper grid used as support in the measurements.

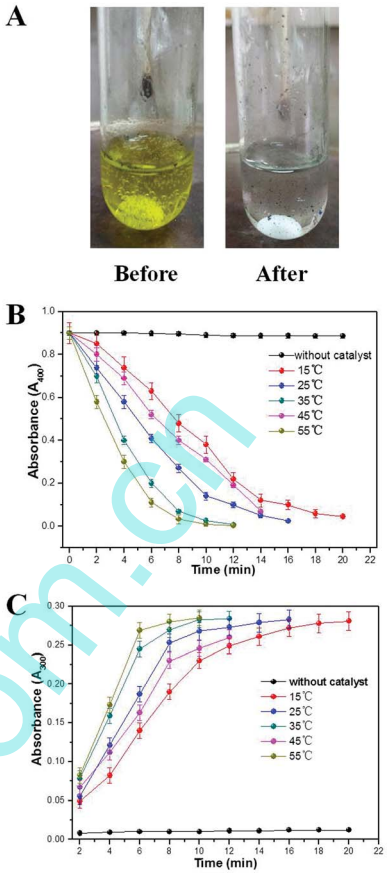

Fig. 4 (A) Catalytic reduction from 4-NP to 4-AP. (B) Reduction of 4-NP in aqueous solution by the GO@PDMAEMA/Au hybrid system at different temperatures recorded by UV-vis spectroscopy. (A_{400} represents absorbance at 400 nm) (C) reduction of 4-NP in aqueous solution recorded by UV-vis spectroscopy every 2 min using the GO@PDMAEMA/Au hybrid system as a catalyst at different temperature. (The absorption peak is 300 nm).

The catalytic reduction of 4-nitrophenol (4-NP) was widely used for testing the activation of the catalyst.[35–37] In this work, the GO@PDMAEMA/Au hybrid was used as a catalyst, and catalytic process was monitored by UV-vis spectroscopy at different temperatures. First of all, Fig. S6† showed the UV-visible spectra of GO, GO@PDMAEMA and GO@PDMAEMA/Au nanocomposites. A strong peak at 230 nm was due to graphene oxide. However, the gold plasmon band at 522 nm was a little weak. The poor surface plasmon of the gold nanoparticles was possibly due to the lower concentration used for the preparation of GO@PDMAEMA/Au. It was important to mention that the lower concentration of gold nanoparticles in the GO@PDMAEMA/Au nanocomposites used in this study gave the best catalytic performance.

When the GO@PDMAEMA/Au hybrid was added into a solution containing 4-NP and $NaBH_4$, the color of the solution changed from yellow green to colorless gradually (Fig. 4A), indicating 4-NP was reduced and changed into 4-aminophenol (4-AP). As 4-NP and 4-AP show different absorption peaks at 400 and 300 nm, respectively, we monitored the intensity of 4-NP at 400 nm to evaluate the catalytic properties of the GO@PDMAEMA/Au hybrid at different temperatures. Without a catalyst, the absorption peak of 4-NP at 400 nm remained unchanged.[38] While, the absorption peak of 4-NP at 400 nm diminished with time in the presence of GO@PDMAEMA/Au, and a new peak at 300 nm appeared due to the formation of 4-AP (Fig. 4B and C and S7†). The high activity arose from the synergistic effect of GO and Au NPs: (1) GO had large specific surface area, which provided much higher probability for Au NPs to touch the 4-NP molecules; and (2) electron transfer from the GO to Au NPs would increase the local electron concentration, greatly facilitating the uptake of electrons by 4-NP molecules.[39]

Kinetic studies at different temperatures demonstrated that the reduction is pseudo-first-order for the loss of 4-NP. Fig. S8† and 5A show the A_t/A_0 and ln (A_t/A_0) *versus* reaction time for the reduction of 4-NP by GO@PDMAEMA/Au, where A_t and A_0 are the peak intensities at time t and 0, respectively. The 4-NP aqueous solution without catalyst showed a negligible catalytic activity with a rate constant of 0.004 min^{-1}. The kinetic rate constant is estimated from the slope to be 0.15, 0.26, 0.51, 0.39 and 0.60 min^{-1} for 15 °C, 25 °C, 35 °C, 45 °C and 55 °C, respectively (Fig. 5A). Fig. 5B demonstrates that the rate constants k obtained at different temperatures do not follow the typical Arrhenius law with constant activation energy.[40] Notably, the apparent rate constants (k) at different temperatures show an obvious turning point in the range 35–45 °C.[41] This expected phenomenon is attributed to the phase transition of grafted PDMAEMA. When environmental temperature is over their LCST, the grafted PDMAEMA chains will undergo a hydrophilic to hydrophobic phase transition, which results in the inclusion

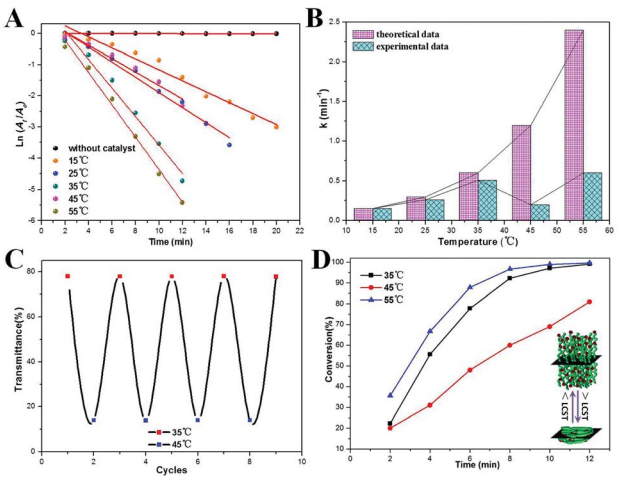

Fig. 5 (A) Plot of $\ln(A_t/A_0)$ *versus* reaction time for the reduction of 4-NP at four different temperatures, (B) the dependence of the apparent rate constant on temperatures. The apparent rate constants (k) at different temperatures show an obvious turning point in the range 35–45 °C, (C) temperature-dependent optical transmittance of GO@PDMAEMA/Au aqueous solutions (0.5 g L^{-1}) *vs.* repeat times. The testing temperature increased or decreased with the initial temperature of 35 °C and (D) The conversion of 4-NP catalyzed by GO@PDMAEMA/Au at different temperatures. GO@PDMAEMA/Au composite particles consisting of thermo-sensitive core–shell particles in which Au NPs are embedded. At high temperature (T > 40 °C), the network shrinks and the catalytic activity of the nanoparticles is strongly affected in this state.

of the Au NPs covered by the collapsed PDMAEMA chains. Therefore, partial catalytically active sites were shielded, and an increased mass transfer resistance is expected. Fig. 5C shows the temperature dependence of optical transmittance of GO@PDMAEMA/Au. The mixture had nearly 80% transmittance at 35 °C. After reaching 45 °C, the transmittance quickly decreased to about 15%. Repeated change of the temperatures around the LCST resulted in repeated changes of the transmittances, as shown in Fig. 5C. It indirectly shows the dispersed status of the same concentration of GO@PDMAEMA/Au in aqueous solutions at 35 °C and 45 °C, respectively. That is to say, GO@PDMAEMA/Au can be uniformly dispersed at 35 °C to result in homogenous suspensions, but it fails to be well dispersed at 45 °C and precipitates quickly. The reason which leads to this phenomenon is that PDMAEMA chains become insoluble and most likely shrink to form hydrophobic aggregates on the surface of GO at high temperature.

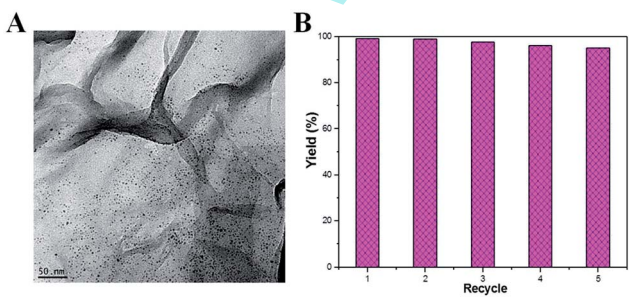

Fig. 6 (A) TEM image of GO@PDMAEMA/Au after the catalytic test. (B) Reusability of GO@PDMAEMA/Au as a catalyst for the reduction of 4-NP with $NaBH_4$.

Many previous studies have reported that the catalyst could still catalyze the reactions at temperatures above the LCST, but with much lower activity.[42] As observed from Fig. 5D, at $T <$ LCST, a homogenous catalyst was found to be more effective for catalytic reduction (35 °C, 6 min, conversion = 78%), whereas at $T >$ LCST, the catalyst was heterogeneous and the reduction rate significantly decreased (45 °C, 6 min, conversion = 48%). This suggested that the hydrophobic shell of PDMAEMA in the GO@PDMAEMA/Au system at a temperature above the LCST just decelerate but not stop the reactants reaching the surface of the gold catalyst. When temperature was further increased, the conversion at 55 °C is at about 87% in 6 min, possibly due to the complete collapse of PDMAEMA chains, limits the diffuse of reactants through the hydrophobic shell.[43] In contrast, under their LCST, the grafted PDMAEMA chains will become hydrophilic, and are completely dissolved in the system, which lead to the 'exposure' of encapsulated Au NPs from PDMAEMA chains. These exposed Au NPs will enhance the catalytic capability.

The structure of GO@PDMAEMA/Au has no change after the catalytic reaction. The Au NPs with the same size distribution (2–3 nm) compared with the catalyst before the reaction were uniformly supported on GO@PDMAEMA sheets (Fig. 6A), indicating that the attachment between Au NPs and GO@PDMAEMA was sufficiently strong. The reusability of catalyst is another important concern. In our system, the GO@PDMAEMA/Au hybrid catalyst system was isolated from the reaction mixture by centrifugation, and reused in the next cycle. As shown in Fig. 6B, the GO@PDMAEMA/Au catalyst can be successfully reused in five repeated processes with a conversion of >95%, indicating excellent recyclability of the catalyst.

Conclusions

In conclusion, we have successfully developed a unique graphene-based smart catalytic system (GO@PDMAEMA/Au) with excellent catalytic performances for temperature adjustable catalysis. This hybrid catalytic system is an effective catalyst for the model reduction of 4-NP to 4-AP in aqueous solution. The catalytic activities of the system can be readily tunable at different temperature windows due to the thermal responsive behavior of PDMAEMA. More work about using various external stimuli, such as light or thermal *etc.* to trigger a pre-designed special smart system for controlling the reaction rates are carried out.

Acknowledgements

This research is supported by Chinese Academy of Science for Hundred Talents Program, Chinese Central Government for Thousand Young Talents Program, the Natural Science Foundation of China (51303195, 51473179, 21304105, 21404110), and Excellent Youth Foundation of Zhejiang Province of China (LR14B040001).

Notes and references

1 S. Stankovich, D. A. Dikin, G. H. B. Dommett, K. M. Kohlhaas, E. J. Zimney, E. A. Stach, R. D. Piner, S. T. Nguyen and R. S. Ruoff, *Nature*, 2006, **442**, 282–286.
2 A. K. Geim and K. S. Novoselov, *Nat. Mater.*, 2007, **6**, 183–191.
3 A. K. Geim, *Science*, 2009, **324**, 1530–1534.
4 L. A. Ponomarenko, F. Schedin, M. I. Katsnelson, R. Yang, E. W. Hill, K. S. Novoselov and A. K. Geim, *Science*, 2008, **320**, 356–358.
5 K. H. Zheng, F. B. Meng, L. Jiang, Q. Y. Yan, H. H. Hng and X. D. Chen, *Small*, 2013, **9**, 2076–2080.
6 J. Liu, X. J. Sun, P. Song, Y. W. Zhang, W. Xing and W. L. Xu, *Adv. Mater.*, 2013, **25**, 6879–6883.
7 H. L. Wang, Y. Y. Liang, M. Gong, Y. G. Li, W. Chang, T. Mefford, J. G. Zhou, J. Wang, T. Regier, F. Wei and H. J. Dai, *Nat. Commun.*, 2012, **3**, 917.
8 T.-K. Hong, D. W. Lee, H. J. Choi, H. S. Shin and B.-S. Kim, *ACS Nano*, 2010, **4**, 3861–3868.
9 C. A. Merchant, K. Healy, M. Wanunu, V. Ray, N. Peterman, J. Bartel, M. D. Fischbein, K. Venta, Z. T. Luo and A. T. C. Johnson, *Nano Lett.*, 2010, **10**, 2915–2921.
10 X. B. Cao, D. P. Qi, S. Y. Yin, J. Bu, F. J. Li, C. F. Goh, S. Zhang and X. D. Chen, *Adv. Mater.*, 2013, **25**, 2957–2962.
11 C. Z. Zhang, N. Mahmood, H. Yin, F. Liu and Y. L. Hou, *Adv. Mater.*, 2013, **25**, 4932–4937.
12 G. M. Scheuermann, L. Rumi, P. Steurer, W. Bannwarth and R. Muülhaupt, *J. Am. Chem. Soc.*, 2009, **131**, 8262–8270.
13 X. M. Chen, G. H. Wu, J. M. Chen, X. Chen, Z. X. Xie and X. R. Wang, *J. Am. Chem. Soc.*, 2011, **133**, 3693–3695.
14 P. Kundu, C. Nethravathi, P. A. Deshpande, M. Rajamathi, G. Madras and N. Ravishankar, *Chem. Mater.*, 2011, **23**, 2772–2780.
15 S. Zhang, Y. Shao, H.-g. Liao, J. Liu, I. A. Aksay, G. Yin and Y. Lin, *Chem. Mater.*, 2011, **23**, 1079–1081.
16 S. Guo, S. Dong and E. Wang, *ACS Nano*, 2009, **4**, 547–555.
17 C. C. Huang, C. Li and G. Q. Shi, *Energy Environ. Sci.*, 2012, **5**, 8848–8868.
18 Y. Y. Liang, H. L. Wang, J. G. Zhou, Y. G. Li, J. Wang, T. Regier and H. J. Dai, *J. Am. Chem. Soc.*, 2012, **134**, 3517–3523.
19 C. Z. Zhang, R. Hao, H. Yin, F. Liu and Y. L. Hou, *Nanoscale*, 2012, **4**, 7326–7329.
20 V. K. Gupta, N. Atar, M. L. Yola, Z. Üstündağ and L. Uzun, *Water Res.*, 2014, **48**, 210–217.
21 Y. Q. Huang, Y. J. Liu, Z. H. Yang, J. L. Jia, X. Li, Y. Luo and Y. P. Fang, *J. Power Sources*, 2014, **246**, 868–875.
22 M. Jahan, Z. L. Liu and K. P. Loh, *Adv. Funct. Mater.*, 2013, **23**, 5363–5372.
23 Z. M. Zhu, X. H. Guo, S. Wu, R. Zhang, J. Wang and L. Li, *Ind. Eng. Chem. Res.*, 2011, **50**, 13848–13853.
24 Y. Lu, Y. Mei, M. Drechsler and M. Ballauff, *Angew. Chem., Int. Ed.*, 2006, **45**, 813–816.
25 J. J. Qi, W. P. Lv, G. H. Zhang, Y. Li, G. L. Zhang, F. B. Zhang and X. B. Fan, *Nanoscale*, 2013, **5**, 6275–6279.
26 E. Z. Zhang, T. Wang, C. X. Lian, W. X. Sun, X. X. Liu and Z. Tong, *Carbon*, 2013, **62**, 117–127.
27 D. R. Wang, G. Ye, X. L. Wang and X. G. Wang, *Adv. Mater.*, 2011, **23**, 1122–1125.
28 T. T. Gao, X. L. Wang, B. Yu, Q. B. Wei, Y. Q. Xia and F. Zhou, *Langmuir*, 2013, **29**, 1054–1060.
29 M. Steenackers, A. Küller, S. Stoycheva, M. Grunze and R. Jordan, *Langmuir*, 2009, **25**, 2225–2231.
30 M. Seifert, A. H. R. Koch, F. Deubel, T. Simmet, L. H. Hess, M. Stutzmann, R. Jordan, J. A. Garrido and I. D. Sharp, *Chem. Mater.*, 2013, **25**, 466–470.
31 P. Xiao, J. C. Gu, J. Chen, J. W. Zhang, R. B. Xing, Y. C. Han, J. Fu, W. Q. Wang and T. Chen, *Chem. Commun.*, 2014, **50**, 7103–7106.
32 Y. J. Chabal, M. Acik, C. Mattevi, C. Gong, G. Lee, K. Cho and M. Chhowalla, *ACS Nano*, 2010, **4**, 5861–5868.
33 W. S. Hummers and R. E. Offeman, *J. Am. Chem. Soc.*, 1958, **80**, 1339.
34 F. H. Li, H. F. Yang, C. S. Shan, Q. X. Zhang, D. X. Han, A. Ivaska and L. Niu, *J. Mater. Chem.*, 2009, **19**, 4022–4025.
35 J. Zeng, Q. Zhang, J. Y. Chen and Y. N. Xia, *Nano Lett.*, 2010, **10**, 30–35.
36 F. Wang, C. H. Li, L. D. Sun, H. S. Wu, T. Ming, J. F. Wang, J. C. Yu and C. H. Yan, *J. Am. Chem. Soc.*, 2011, **133**, 1106–1111.
37 Z. Jin, M. D. Xiao, Z. H. Bao, P. Wang and J. F. Wang, *Angew. Chem., Int. Ed.*, 2012, **51**, 6406–6410.
38 Y. Shin, A. Dohnalkova and Y. H. Lin, *J. Phys. Chem. C*, 2010, **114**, 5985–5989.
39 J. Li, C. Y. Liu and Y. Liu, *J. Mater. Chem.*, 2012, **22**, 8426–8430.
40 R. C. Cáceres, A. S. Iglesias, M. Karg, I. P. Santos and J. P. Juste, *Adv. Mater.*, 2008, **20**, 1666–1670.
41 S. Wu, J. Dzubiella, J. Kaiser, M. Drechsler, X. H. Guo, M. Ballauff and Y. Lu, *Angew. Chem., Int. Ed.*, 2012, **51**, 2229–2233.
42 X. W. Jiang, D. A. Xiong, Y. L. An, P. W. Zheng, W. Q. Zhang and L. Q. Shi, *J. Polym. Sci., Part A: Polym. Chem.*, 2007, **45**, 2812–2819.
43 F. P. Dong, W. P. Guo, S. K. Park and C. S. Ha, *Chem. Commun.*, 2012, **48**, 1108–1110.